Carbon 233 (2025) 119852

Contents lists available at ScienceDirect

Carbon

journal homepage: www.elsevier.com/locate/carbon

Self-healing kinetics in monolayer graphene following very low energy ion irradiation

P. Vinchon [a,b,*], S. Hamaguchi [b], S. Roorda [a], F. Schiettekatte [a], L. Stafford [a]

[a] Département de Physique, Université de Montréal, Montréal, Québec, Canada
[b] Graduate School of Engineering, Osaka University, Osaka, 565-0871, Japan

A B S T R A C T

Monolayer graphene subjected to 13 and 90 eV Ar ion irradiation was probed by in-situ Raman spectroscopy. At 90 eV ion irradiation, a simple damage accumulation is seen. However, at 13 eV, immediately after damage formation, significant graphene self-healing is observed in real time. We argue that energy deposition through very-low-energy ion collisions can create vacancies and carbon adatoms which can diffuse easily on the surface and recombine afterward. The self-healing kinetics exhibit a fast (~10 s) and a slow regime (~30 min), which cannot result only from adatom-vacancy recombination. Based on a defect kinetic model, self-healing efficiency is revealed to be limited by dimer formation. Yet, the interplay between Stone-Wales defects and adatoms enables progressive release of the latter, and subsequent graphene self-healing on a longer time scale.

1. Introduction

Defect engineering of monolayer graphene is an essential strategy for the implementation of this material in various applications [1–4]. Atomic scale defects can be generated in pristine graphene by high-energy ion or electron beam irradiations [5–7]. Such experiments demonstrated an energy threshold for defect generation at $T_d = 18 - 22$eV [7–9], in agreement with first-principle calculations [7,10] and molecular dynamics (MD) simulations [11]. Nevertheless, while high-energy ions (>90 eV) lead to sputtering of carbon atoms, and thus to vacancies in the graphene lattice, defects can also be created by very-low-energy ions (10–15 eV) irradiation [12–14]. Compared to electron beam irradiation, ion-surface interactions are more complex [10,14] and several experiments reveal that they can produce defects below the traditional value of T_d [12–14]. Here, potential energy released from ion neutralization (for example, 15.76 eV for single charged argon ions) at the point of impact combined with ion's kinetic energy could provide enough energy to generate the experimentally observed vacancy-like defects. Another potential path for defect generation could involve impurities remaining in low-pressure vacuum chambers. In all cases, a full understanding of the physics driving defect generation by sub-threshold ions is still lacking. Since incident particle kinetic energy is significantly lower than T_d, carbon adatoms are expected to remain on the graphene surface and to easily migrate at room temperature. Hence, they can encounter other 0D or 1D defects (such as grain boundaries (GBs)), resulting in adatoms-vacancies recombination. As a result, preferential self-healing at GBs has been recently observed [15]. Defect healing in graphene domains was investigated both experimentally and theoretically for some specific cases [16,17]. Such studies have revealed that defect healing of graphene requires annealing at high temperatures and the introduction of additional carbon sources [18–23] such as PMMA residues or hydrocarbon impurities. Since graphene characterization is typically performed at atmospheric pressure, real-time monitoring of the formation, migration, and annihilation of defects during irradiation or plasma processing has been difficult to achieve so far.

In this work, we report evidence of defects self-healing in monolayer graphene by adatoms from vacancies generated by very-low-energy ion irradiation. An experimental setup dedicated to the study of plasma-surface interactions [24] is used to assess the influence of such ions on graphene in real time. Graphene is analyzed using *in-plasma* Raman spectroscopy, during and after ion beam exposure. Careful examination of the Raman spectra allows to track the increase of vacancy-like defect (VLD) concentration during ion irradiation. While a simple damage accumulation is seen for high-energy irradiation, an abrupt decrease is observed immediately after damage formation through bombardment by very-low-energy species, followed by a slower self-healing process. As carbon adatoms generated by very-low-energy ion irradiation can diffuse on the graphene surface, they can recombine with vacancies. However, they may also react with other adatoms, resulting in the formation of dimers. Furthermore, they can catalytically promote the healing of Stone-Wales (SW) defects without being integrated into the

* Corresponding author. Graduate School of Engineering, Osaka University, Osaka, 567-0871, Japan.
E-mail address: vinchon@ppl.eng.osaka-u.ac.jp (P. Vinchon).

https://doi.org/10.1016/j.carbon.2024.119852
Received 14 August 2024; Received in revised form 18 November 2024; Accepted 21 November 2024
Available online 22 November 2024

graphene lattice [25,26]. This study demonstrates that real-time monitoring of 2D materials during and after very-low-energy ion exposure can provide important information about their kinetics, that will benefit applications, including any post-treatment methods involving ion and plasma processes such as substitutional doping [27–29].

2. Material and methods

A detailed description of the experimental setup used herein is provided in Ref. [24]. Briefly, the setup is equipped with an inductively coupled plasma source composed of a helical-shaped antenna. A power of 50W is applied to generate an RF Ar plasma at a pressure of 5 mTorr (Plasmionique Inc.). Two grids at its exit are used to generate the low-energy ion beam: a DC voltage is applied to the first while the second is grounded.

Monolayer graphene samples are grown on 25-µm copper substrates by Chemical Vapor Deposition (CVD) [30]. Graphene is transferred to 1 cm^2 Si/SiO_2 by using a standard transfer procedure with poly(methylmethacrylate) (PMMA) [28].

Raman analyses are conducted at a 532 nm wavelength and 1 W maximal power. Considering that the area probed by each optical beam spot is 8 µm wide, the power density is estimated at 0.33 mW/$µm^2$ over each spot [24]. This is well below the threshold energy needed to generate defects in graphene [30]. A Lorentzian function is used to fit each Raman peak from monolayer graphene, such as the D (1325 cm^{-1}), G (1575 cm^{-1}), D' (1610 cm^{-1}), and 2D (2675 cm^{-1}). Throughout this manuscript, the notation *I* correspond to the peak height obtained after fitting. Measurements are taken every 10 s, with an integration time of 4 s and avoiding laser irradiation of graphene with a shutter during the next 6 s. Typical Raman spectra are presented in Supplementary Section II.

3. Results

To mimic the conditions of low-energy ion bombardment on unbiased surfaces exposed to low-pressure plasmas (ions are accelerated through a low-voltage plasma sheath), the ion energy is set at 13 eV. The graphene film is exposed to five successive cycles consisting of an ion beam exposure lasting around 2 min followed by a 30-min interval during which the pressure reaches 4×10^{-7} Torr. In the meantime, an *in-plasma* Raman system is used to simultaneously monitor 9 different spots scattered over a 1.6 × 1.6 mm^2 area on the graphene surface. Experiments resulted in a total of 45 Raman time series (9 spots × 5 cycles). As presented in supplementary Section I, the influence of Raman measurements on the studied phenomenon has been deemed negligible in the low-defect concentration regime. For clarity, the evolution of only one representative spot is shown in the rest of the paper, but all spots were considered in the analysis. To gain insight into defect concentration evolution, intensity ratios of D-to-G peaks (I_D/I_G) and D-to-2D (I_D/I_{2D}) peaks are examined [15,31,32]. The time evolution of these ratios is presented in Fig. 1. For every cycle, both ratios increase during ion beam irradiation and decrease as soon as the ion beam is turned off. This sharp drop occurs over the first 30 s in the post-processing period, then the decrease rate slows down for both ratios. Values of I_D/I_G gradually increase with cycle numbers from 0.1 to 3.5, indicating that graphene remains in the low defect concentration domain [33]. From Fig. S3 (Supplementary Section III), values of D-to-D' ratio ($I_D/I_{D'}$) remains close to 7 for all subsequent plasma treatment, corresponding to VLD. Hence, it appears that sub-threshold ion irradiation results in the production of VLDs. Starting from the 3rd cycle, an initial burst and subsequent decrease in I_D/I_G and I_D/I_{2D} during the first moments of processing can be observed. This can be linked to a sudden burst of current measured at the sample holder when the shutter is open at the beginning of experiments. This implies that a temporary increase in ion flux is obtained, which can generate a high number of defects in the first moments of exposure. As ion flux decreases gradually to reach steady

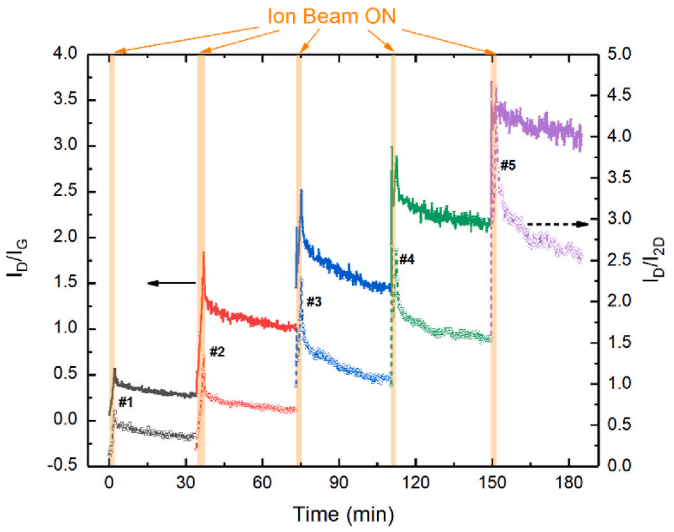

Fig. 1. Time evolution of I_D/I_G (full markers) and I_D/I_{2D} (empty markers) during five subsequent cycle of ion beam exposure (yellow bands) and subsequent 30 min pause. (For interpretation of the references to colour in this figure legend, the reader is referred to the Web version of this article.)

state, all adatoms removed from the lattice can diffuse and heal a portion of VLDs. This results in a decrease in the next 20 s before switching again to a rise of peaks ratio. Overall, the results indicate that, after exposure to low-energy ion irradiation, both I_D/I_G and I_D/I_{2D} ratios exhibit two different decay behaviors: i) a sharp decrease (observed immediately after shutting off the ion beam), followed by ii) a much slower decrease. The similarity of the trends for the two ratios reveals that defect concentration decreases naturally over time at room temperature following low-energy ion irradiation. While both ratios, I_D/I_G and I_D/I_{2D}, present similar behaviors, the latter is unaffected by either the doping or stress level of the graphene sheet [34,35]. I_D/I_{2D} will henceforth be considered as the main indicator of VLD concentration.

To assess the effect of ion energy on the self-healing process, graphene samples were also exposed to 90 eV ions, as in Ref. [33]. Fig. 2 compares the I_D/I_{2D} evolution profiles of graphene samples exposed to

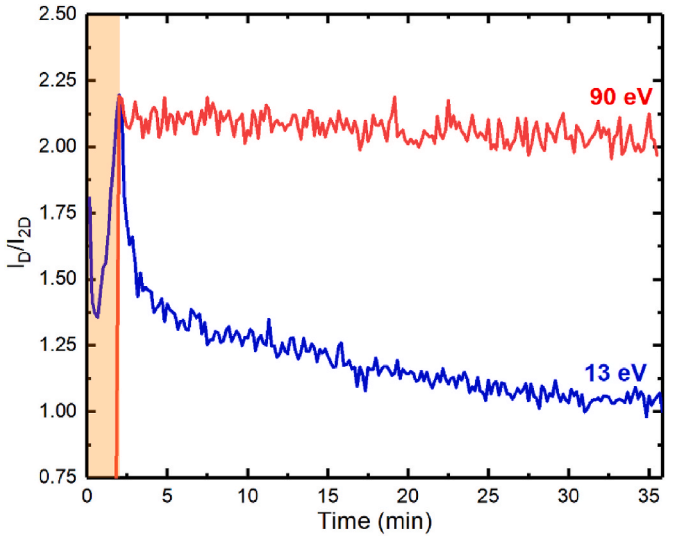

Fig. 2. Temporal evolution of the I_D/I_{2D} intensity ratio during and after exposure to 13 eV (blue curve) and 90 eV (red curve) ion beams. The time scales have been shifted so that the end times of ion irradiation in both cases coincide. (For interpretation of the references to colour in this figure legend, the reader is referred to the Web version of this article.)

13 and 90 eV ion beams. During irradiation by 13 eV ions, the I_D/I_{2D} ratio presents the same initial increase and decrease phenomenon observed on Fig. 1 before it rises to a maximum of 2.2 after 120 s. Once irradiation is stopped, the ratio quickly drops to 1.5 in the first 60 s and then slowly reaches 1.08 after 30 min. When the ion energy is set to 90 eV, defect generation occurs as expected much faster, and an I_D/I_{2D} ratio of 2.2 is reached within 30 s only. In the post-irradiation period, the ratio remains fairly constant. This indicates that while the graphene defects induced by low-energy ion exposure (13 eV) can self-heal in the post-irradiation period, those induced by higher-energy ion exposure cannot.

When the energy of the incoming ions is high, carbon atoms are sputtered away from the graphene sheet [5], which suppresses any possible self-healing. Therefore, the results obtained herein reveal that self-healing is mediated by the carbon adatoms produced during low-energy ion irradiation. As soon as the irradiation stops, the adatoms partly recombine with VLD created during processing, thereby reestablishing the graphene structure. Furthermore, the shape of the decreasing profiles varies depending on the number of ion-exposure cycles (Fig. 1). As shown in Fig. S4 (Supplementary Section IV), the decrease cannot solely result from a second-order reaction such as adatoms-vacancy recombination. Hence, several mechanisms must influence graphene self-healing, which probably depends on the concentration of graphene defects.

4. Discussions

4.1. Self-healing mechanisms

A mechanism of graphene defect formation and self-healing is proposed in Fig. 3. From now on, VLDs are assumed to be monovacancy. The different steps presented in Fig. 3a, b, and 3c are related to Fig. 3d which present vacancy concentration as a function of time. The latter can be obtained through its linear relationship with I_D/I_{2D} [33]. First, carbon adatoms are generated from the graphene sheet upon exposure to low-energy ion irradiation (Fig. 3a), thereby creating vacancies (#1.1). The generated adatoms can diffuse on the graphene surface and will be essential afterward for graphene self-healing. On the other hand, SW defects may also be induced by ion beam exposure (#1.2) and/or formed upon imperfect vacancy-adatom recombination [36]. These defects involve in-plane bond rotations with no loss of carbon atoms and are constituted of two pentagons and two heptagons instead of the classical hexagons [7]. Due to their relatively low formation energy (10 eV), even low-energy ions are expected to generate a non-negligible amount of such defects at room temperature. Furthermore, since the activation energy for recovery is high (5.5 eV), the healing of such defects at room temperature is unlikely.

Once the ion beam is turned off, no more defects can be formed (Fig. 3b), and the adatoms diffusing on the surface can eventually recombine with vacancies (#2.1), resulting in the fast defect concentration decrease observed in Fig. 3d. Adatoms can also very easily combine with other adatoms to form dimers (#2.2), which are stable at room temperature. As detailed in the next section, the dimerization of adatoms is the main obstacle impeding complete graphene recovery.

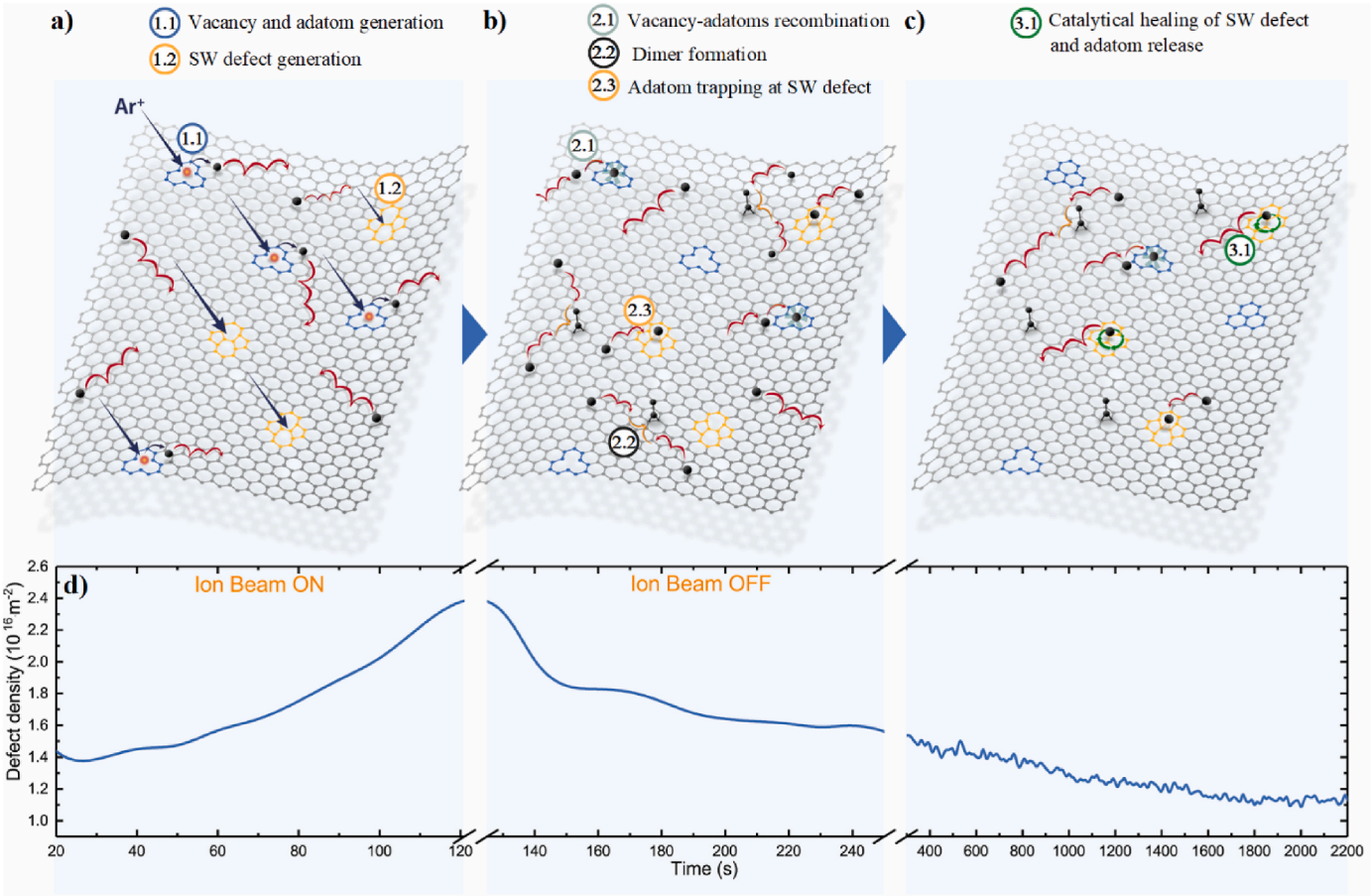

Fig. 3. Illustration of the dynamic processes occurring on the graphene surface during a) ion bombardment, b) immediately after shutting off the ion beam, and c) later in the post-irradiation period. d) Plot shows defect density as a function of time corresponding to each step.

Fig. 3c focuses on graphene evolution later in the post-irradiation period (>400 s). As presented in Fig. 3d, the rate of decrease in I_D/I_{2D} slows down but remains significant. Vacancy healing at this timescale indicates that some adatom recombination with defects is delayed. Catalytic healing of SW defects by carbon adatoms is expected to take place (#3.1) and act as a temporary trap for adatoms. Indeed, the activation energy for SW healing at room temperature greatly decreases from 5.5 eV to 0.86 eV once a carbon adatom reaches the center of the defect [25,26]. Still, since the activation energy remains high, adatoms are trapped at SW defects for a significant amount of time (#2.3). Interestingly, an adatom is re-emitted after catalytic healing and can diffuse again freely over the graphene surface until it encounters a vacancy, another carbon adatom, or another SW defect. Considering that the sensitivity of the Raman spectroscopy technique to SW defects is low [37], it is not possible to link the decrease in I_D/I_{2D} ratio to SW healing. However, it can indirectly be related to SW healing by the re-emission of adatoms, which then recombine with vacancies.

4.2. Kinetic model

To confirm the applicability of the proposed mechanism, a kinetic model for the time evolution of defect concentration after low-energy ion irradiation is proposed. It consists of a system of differential equations describing the interrelated time evolution of the concentration C of six species presented below. A distinction is made between free adatoms able to diffuse on the graphene surface (C_a) from adatoms trapped in the vicinity of SW defects (Trap #1 – C_{T1}) at rate k_{T1}, depending on the concentration of SW defects (C_{sw}). An adatom in Trap #1 can then either escape away from SW defects back to pristine graphene at a rate K_{esc} or get further trapped at the center of the SW defects (Trap #2 – C_{T2}) at rate K_{T2}.The latter can then initiate SW defects catalytic healing at a rate K_{cat}. Free adatoms can also form dimers (C_{di}) at rate k_{di}, or recombine with vacancies (C_v) at rate k_v.

On one hand, second-order reactions (rate k_x) directly influenced by adatoms diffusion on graphene's surface are considered as well as first-order reactions (rate K_x). Such reactions as SW defects healing by adatoms in trap#2 (C_{T2}) are not influenced directly by adatoms diffusion. Second-order rates are determined as follows:

$$k_x = D\exp(-E_x / k_B T), \tag{1}$$

where E_x is the activation energy for the reaction, k_B is the Boltzmann constant, T is the graphene temperature, assumed to be 300 K, and D is the adatom diffusion coefficient given by:

$$D = \frac{1}{4}(d)^2 \omega_{ph} \exp\left(-E_a / k_B T\right), \tag{2}$$

where $\omega_{ph} = 4.8 \times 10^{13}$ Hz is the graphene maximal phonon frequency, $d = 1.6$ Å is the adatoms jump length, and E_a the activation energy for carbon adatom diffusion on graphene. E_a values are allowed to vary to better fit experimental data between 0.4 eV and 0.5 eV as this range is commonly found in the literature. The use of a lower value down to 0.3 eV determined recently [38] does not enable to fit experimental data, unless the prefactor of Eq. (2) is an order of magnitude smaller. On the other hand, first-order reaction rates can be determined as:

$$K_x = \omega_{ph} \exp(-E_x / k_B T). \tag{3}$$

Table 1
Activation energy used in the kinetic model for adatom vacancy recombination k_v, initial adatom trapping at SW defects k_{T1}, adatom escape from initial trapping K_{esc}, dimer formation k_{di}, adatom trapping at the center of SW defects K_{T2} and catalytically healing of SW defects K_{cat}.

	k_v	k_{T1}	K_{esc}	k_{di}	K_{T2}	K_{cat}
E_x (eV)	0.24 [39,40]	0.23 [22]	0.71 [22]	0.25 [41]	0.6	0.97

Activation energy values used in the model are summarized in Table 1.

Note that, to correctly model the C_v decrease over time, E_{T2} and E_{cat} values are different from those given by Wang et al. of 0.98 eV and 0.86 eV, respectively [25]. Indeed, a high activation energy for K_{T2} would lead to a very low rate of adatoms trapping at SW defects and thus have a weak influence on graphene self-healing. As for the SW defect healing rate K_{cat}, it directly influences the slower decrease of C_v at larger timescales. Even though the obtained value of E_{cat} is higher than the one reported previously (0.8–0.86 eV [25,26]), it is close enough considering the model simplicity. To the best of our knowledge, no values of E_{di} has been reported for carbon adatoms on graphene; a value of $E_{di} = 0.25$eV obtained for carbon dimer formation on copper is used [41].

At time $t = 0$, a population of free adatoms (C_a) able to diffuse on the graphene surface can recombine with vacancies (C_v), at rate k_v, form dimers at rate k_{di}, or be trapped in Trap #1 in the vicinity of SW defects (C_{sw}) at rate k_{T1}. So C_a evolve at a rate:

$$\frac{dC_a}{dt} = -k_v C_a C_v - k_{T1} C_a C_{sw} + K_{esc} C_{T1} - 2k_{di} {C_a}^2 + K_{cat} C_{T2} \tag{1}$$

where the second term on the right-hand side represents the adatom escaping from the concentration already trapped in Trap #1, C_{T1}. This concentration evolves as:

$$\frac{dC_{T1}}{dt} = k_{T1} C_a C_{sw} - K_{esc} C_{T1} - K_{T2} C_{T1} \tag{2}$$

where the first two terms on the right-hand side were found, with opposed sign, in Eq. (1), and the last term represents the number of adatoms going from Trap #1, in the vicinity of the SW defects, to Trap #2 at the center of the SW defects. The concentration of adatoms trapped there, C_{T2}, evolves as

$$\frac{dC_{T2}}{dt} = K_{T2} C_{T1} - K_{cat} C_{T2} \tag{3}$$

where the first member on the right hand is in Eq. (2) with an opposite sign, and the last term represents the catalytic healing of the SW defect by the adatoms trapped in Trap #2. As a result, the population of SW defects therefore evolves as

$$\frac{dC_{sw}}{dt} = -K_{cat} C_{T2}. \tag{4}$$

Finally, from the first and last terms of the right-hand side of Eq. (1), we get correspondingly that the dimer population should evolve as

$$\frac{dC_{di}}{dt} = k_{di} {C_a}^2 \tag{5}$$

and that of the vacancies as

$$\frac{dC_v}{dt} = -k_v C_a C_v. \tag{6}$$

This last equation gives us the evolution of the vacancy concentration. It can be directly compared to the experimental vacancy concentration using the proportional relationship between the latter and the I_D/I_{2D} Raman signal ratio extracted from Ref. [33]. Fig. 4 presents the time evolution of vacancies, free carbon adatoms, trapped carbon adatoms, SW defects, and carbon dimers concentration obtained from the kinetic model, in addition to the experimental data for vacancy concentration after the 1st ion beam irradiation.

The initial values of experimental and simulated defect densities (C_{v0}) were both set equal at 5.7×10^{15} m^{-2}, while C_{a0} and C_{sw0} were set at 3.7×10^{15} m^{-2} and 2.5×10^{15} m^{-2}, respectively, to obtain the best fit. We note that the initial value of C_v is ~10^4 times smaller than the typical ion fluence received by a surface exposed to a low-pressure Ar plasma (~10^{19} ions.m^{-2}.s^{-1} [12]), i.e. the generation of VLDs by 13 eV Ar ions is a rare event. Within 70 s, the experimental defect density decreases

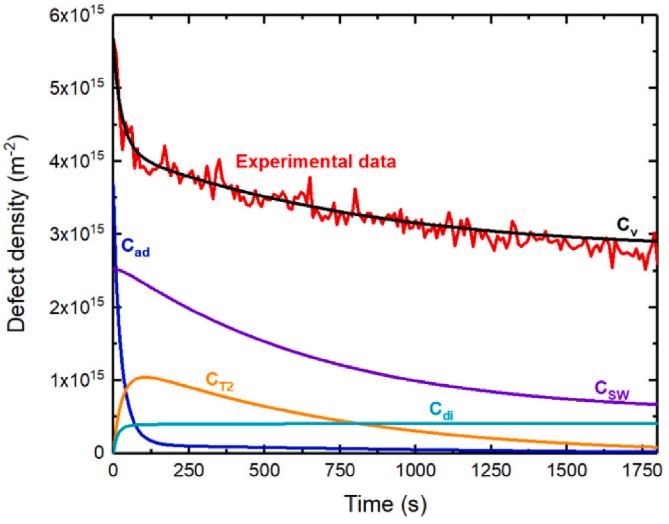

Fig. 4. Temporal evolution of simulated vacancy C_v (black), free adatom Ca (blue), adatom in trap#2 CT2 (orange), SW defect C_{sw} (purple), and dimers C_{di} (cyan) densities, as well as the experimental vacancy density (red). Note that adatom density in trap#1 is too low to be presented here but can be seen in a logarithmic plot in Supplementary Section V. (For interpretation of the references to colour in this figure legend, the reader is referred to the Web version of this article.)

sharply to 3.9×10^{15} m^{-2}, and similar behavior is observed for C_v in the kinetic model. The agreement between the experimental and modeled defect evolution is maintained in the slow decrease period, and the densities fall to 2.8×10^{15} m^{-2} after 30 min. Interestingly, in the model, C_a abruptly decreases to 1.2×10^{15} m^{-2} within 40 s, then it decreases slowly to reach 1.4×10^{13} m^{-2} at the end of the analysis (30 min). The fast decrease is mainly due to direct vacancy healing, as well as dimer formation, when the adatom density is high. Indeed, in the model, the dimer concentration increases sharply to 3.8×10^{14} m^{-2} within 60 s, then it increases gradually to 4.1×10^{14} m^{-2} after 30 min. As for the concentration of trapped adatoms in SW defects (Trap#2), it increases quickly to reach a maximum of 1×10^{15} m^{-2} after only 2 min, then it decreases to 6.9×10^{13} m^{-2} after 30 min. The decrease is related to the catalytic healing of SW defects as C_{sw} decreases throughout the experiment, reaching 6.5×10^{14} m^{-2} at the end.

Overall, the simulation results show that the kinetic model proposed herein can reproduce very well the experimentally observed decrease in defect density. The close agreement between our kinetic model fits and the experimental data lends credence to the mono-vacancy assumption Moreover, free adatoms are rapidly consumed in vacancy healing, as well as in dimerization reaction and SW defect trapping. The adatom released from the catalytic SW defect healing process may then participate in vacancy healing, among other processes. However, since the activation energy of adatom diffusion is low (0.4–0.5 eV), the recovery of vacancies is fast, albeit incomplete. This is mostly attributed to dimerization, as predicted by MD simulations [20]. To confirm the validity of the kinetic model, it is used to simulate defect concentration obtained from the time evolution of I_D/I_{2D} at the remaining eight experimentally probed locations on the graphene surface, for all five treatments. It was possible to correctly fit all 45 curves (with $R^2 > 0.95$) by keeping the parameters presented in Table 1 constant. Supplementary Section VI presents the evolution of the three fitting parameters: C_{a0}, C_{sw0}, and E_a. Interestingly, for a given irradiation treatment, the fitting parameters for each Raman point are similar. For all five cycles, fitting parameters remains around $0.7 \times C_{v0}$ for C_{a0}, $0.3 \times C_{v0}$ for C_{sw0}, while E_a gradually increases from 0.4 to 0.5 eV.

5. Conclusion

This study investigates the effect of low-energy (13 and 90 eV) ion-irradiation on defect formation and self-healing in monolayer graphene films. Experimental analyses are conducted during and immediately after ion bombardment using *in-plasma* Raman spectroscopy. The results demonstrate that the defect concentration determined using the I_D/I_{2D} intensity ratio increases during irradiation with 13 eV argon ions, and it decreases significantly over a few minutes once the ion beam is shut off. However, almost no decrease is observed when graphene is exposed to 90 eV argon ions; this demonstrates that carbon adatoms play a crucial role in graphene healing at room temperature. Indeed, the proposed kinetic model confirms that at room temperature, the defect concentration drops suddenly after the end of the irradiation due to the fast diffusion and recombination of adatoms with vacancies. However, adatoms may combine with other adatoms, resulting in the formation of dimers, which restricts the complete self-healing of graphene. In addition, adatoms may be trapped in SW defects. This process does not significantly impede graphene healing, since the adatoms are released after participating in catalytic SW defect healing; however, it explains the slow vacancies' healing rate observed at longer times, due to the relatively high activation energy of the process. Indeed, as adatoms are released, they may recombine with vacancies but also be trapped in other SW defects, or form dimers.

Those results show how crucial post-treatment surface phenomena are in monolayer graphene processing by techniques involving sub-threshold energy ions such as plasma treatment. This calls for a broadened use of *in-plasma* characterization techniques to ensure the full understanding of phenomena ongoing during or immediately after material modification. This is specifically important for defect engineering of monolayer graphene, and potentially, other 2D materials.

CRediT authorship contribution statement

P. Vinchon: Writing – review & editing, Writing – original draft, Visualization, Validation, Software, Methodology, Investigation, Formal analysis, Data curation. **S. Hamaguchi:** Writing – review & editing, Validation, Methodology, Formal analysis. **S. Roorda:** Writing – review & editing, Supervision, Resources, Investigation, Funding acquisition, Formal analysis, Conceptualization. **F. Schiettekatte:** Writing - review & editing, Validation, Supervision, Resources, Project administration, Methodology, Investigation, Funding acquisition, Conceptualization. **L. Stafford:** Writing – review & editing, Validation, Supervision, Resources, Project administration, Investigation, Funding acquisition, Conceptualization.

Declaration of competing interest

The authors declare that they have no known competing financial interests or personal relationships that could have appeared to influence the work reported in this paper.

Acknowledgment

This work was financially supported by the Canada Foundation for Innovation (CFI), the National Science and Engineering Research Council (NSERC), the Fonds de recherche du Québec - Nature et Technologie (FRQNT) through the Regroupement québécois sur les matériaux de pointe (RQMP), and Japan Society for the Promotion of Science (JSPS). The authors would like to thank Fabrice Debris and Martin Chicoine for their technical help and advice. The authors would also like to thank Prof. Martel for providing high-quality monolayer graphene samples.

Appendix A. Supplementary data

Supplementary data to this article can be found online at https://doi.org/10.1016/j.carbon.2024.119852.

References

[1] J.H. Kim, J.H. Hwang, J. Suh, S. Tongay, S. Kwon, C.C. Hwang, J. Wu, J.Y. Park, Work function engineering of single layer graphene by irradiation-induced defects, Appl. Phys. Lett. 103 (2013) 171604, https://doi.org/10.1063/1.4826642.

[2] W. Zhao, Y. Wang, Z. Wu, W. Wang, K. Bi, Z. Liang, J. Yang, Y. Chen, Z. Xu, Z. Ni, Defect-Engineered heat transport in graphene: a route to high efficient thermal rectification, Sci. Rep. 511962 (2015), https://doi.org/10.1038/srep11962.

[3] M. Schleberger, J. Kotakoski, 2D material science: defect engineering by particle irradiation, Materials 11 (2018) 1885, https://doi.org/10.3390/ma11101885.

[4] J. Liu, Z. Liu, C.J. Barrow, W. Yang, Molecularly engineered graphene surfaces for sensing applications: a review, Anal. Chim. Acta 859 (2015) 1–19, https://doi.org/10.1016/j.aca.2014.07.031.

[5] M.M. Lucchese, F. Stavale, E.H.M. Ferreira, C. Vilani, M.V.O. Moutinho, R. B. Capaz, C.A. Achete, A. Jorio, Quantifying ion-induced defects and Raman relaxation length in graphene, Carbon 48 (2010) 1592–1597, https://doi.org/10.1016/j.carbon.2009.12.057.

[6] C. Su, M. Tripathi, Q.-B. Yan, Z. Wang, Z. Zhang, C. Hofer, H. Wang, L. Basile, G. Su, M. Dong, J.C. Meyer, J. Kotakoski, J. Kong, J.-C. Idrobo, T. Susi, J. Li, Engineering single-atom dynamics with electron irradiation, Sci. Adv. 5 (2019) eaav2252, https://doi.org/10.1126/sciadv.aav2252.

[7] F. Banhart, J. Kotakoski, A.V. Krasheninnikov, Structural defects in graphene, ACS Nano 5 (2011) 26–41, https://doi.org/10.1021/nn102598m.

[8] F. Banhart, Irradiation effects in carbon nanostructures, Rep. Prog. Phys. 62 (1999) 1181–1221, https://doi.org/10.1088/0034-4885/62/8/201.

[9] T. Susi, C. Hofer, G. Argentero, G.T. Leuthner, T.J. Pennycook, C. Mangler, J. C. Meyer, J. Kotakoski, Isotope analysis in the transmission electron microscope, Nat. Commun. 7 (2016) 13040, https://doi.org/10.1038/ncomms13040.

[10] S. Kretschmer, S. Ghaderzadeh, S. Facsko, A.V. Krasheninnikov, Threshold ion energies for creating defects in 2D materials from first-principles calculations: chemical interactions are important, J. Phys. Chem. Lett. 13 (2022) 514–519, https://doi.org/10.1021/acs.jpclett.1c03995.

[11] E.P. Bellido, J.M. Seminario, Molecular dynamics simulations of ion-bombarded graphene, J. Phys. Chem. C 116 (2012) 4044–4049, https://doi.org/10.1021/jp208049t.

[12] P. Vinchon, X. Glad, G. Robert-Bigras, R. Martel, A. Sarkissian, L. Stafford, A combination of plasma diagnostics and Raman spectroscopy to examine plasma-graphene interactions in low-pressure argon radiofrequency plasmas, J. Appl. Phys. 126 (2019) 233302, https://doi.org/10.1063/1.5125143.

[13] R. Villarreal, P.-C. Lin, Z. Zarkua, H. Bana, H.-C. Tsai, M. Auge, F. Junge, H. Hofsäss, E. Tosi, S.D. Feyter, S.D. Gendt, S. Brems, E.H.Å. hlgren, L.M.C. Pereira, Bond defects in graphene created by ultralow energy ion implantation, Carbon 203 (2023) 590–600, https://doi.org/10.1016/j.carbon.2022.12.005.

[14] M. Tripathi, A. Markevich, R. Böttger, S. Facsko, E. Besley, J. Kotakoski, T. Susi, Implanting germanium into graphene, ACS Nano 12 (2018) 4641–4647, https://doi.org/10.1021/acsnano.8b01191.

[15] P. Vinchon, X. Glad, G. Robert Bigras, R. Martel, L. Stafford, Preferential self-healing at grain boundaries in plasma-treated graphene, Nat. Mater. 20 (2021) 49–54, https://doi.org/10.1038/s41563-020-0738-0.

[16] J. Chen, T. Shi, T. Cai, T. Xu, L. Sun, X. Wu, D. Yu, Self healing of defected graphene, Appl. Phys. Lett. 102 (2013) 103–107, https://doi.org/10.1063/1.4795292.

[17] R. Zan, Q.M. Ramasse, U. Bangert, K.S. Novoselov, Graphene reknits its holes, Nano Lett. 12 (2012) 3936–3940, https://doi.org/10.1021/nl300985q.

[18] T. Botari, R. Paupitz, P.A. da S. Autreto, D.S. Galvao, Graphene healing mechanisms: a theoretical investigation, Carbon 99 (2016) 302–309, https://doi.org/10.1016/j.carbon.2015.11.070.

[19] K. Vijayasekhar, S.G. Acharyya, S. Debroy, V.P.K. Miriyala, A. Acharyya, Self-healing phenomena of graphene: potential and applications, Open Phys. 14 (2016) 364–370, https://doi.org/10.1515/phys-2016-0040.

[20] L. Wang, F. Duan, Healing mechanism of multi-vacancy defective graphene under carbon irradiation, Fullerenes, Nanotub. Carbon Nanostruct. 27 (2019) 247–255, https://doi.org/10.1080/1536383X.2019.1566223.

[21] K.V. Zakharchenko, A.V. Balatsky, Controlled healing of graphene nanopores, Carbon 80 (2014) 12–18, https://doi.org/10.1016/j.carbon.2014.07.085.

[22] U. Khalilov, M. Yusupov, G.B. Eshonqulov, E.C. Neyts, G.R. Berdiyorov, Atomic level mechanisms of graphene healing by methane-based plasma radicals, FlatChem 39 (2023) 100506, https://doi.org/10.1016/j.flatc.2023.100506.

[23] O. Dyck, J. Swett, A. Lupini, S. Jesse, Super-graphene: the role of temperature on radiation resistance, Microsc. Microanal. 26 (2020) 2360–2361, https://doi.org/10.1017/S1431927620021327.

[24] P. Vinchon, S. Asadollahi, C. Côté, S. Marcet, Stephane E. Atallah, É. Dessureault, M. Chicoine, A. Sarkissian, R. Leonelli, S. Roorda, F. Schiettekatte, L. Stafford, In-plasma analysis of plasma-surface interactions, Rev. Sci. Instrum. 94 (2023) 083305, https://doi.org/10.1063/5.0130235.

[25] C. Wang, Y.H. Ding, Catalytically healing the Stone-Wales defects in graphene by carbon adatoms, J. Mater. Chem. A 1 (2013) 1885–1891, https://doi.org/10.1039/c2ta00736c.

[26] G.D. Lee, G.D. Lee, A.W. Robertson, S. Lee, Y.C. Lin, J.W. Oh, H. Park, Y.C. Joo, Y. C. Joo, E. Yoon, K. Suenaga, J.H. Warner, C.P. Ewels, Direct observation and catalytic role of mediator atom in 2D materials, Sci. Adv. 6 (2020) eaba4942, https://doi.org/10.1126/sciadv.aba4942.

[27] G.R. Bigras, X. Glad, P. Vinchon, R. Martel, L. Stafford, Selective nitrogen doping of graphene due to preferential healing of plasma-generated defects near grain boundaries, npj 2D Materials and Applications 4 (2020) 42, https://doi.org/10.1038/s41699-020-00176-y.

[28] P. Vinchon, X. Glad, G. Robert-Bigras, R. Martel, A. Sarkissian, L. Stafford, Postgrowth modification of monolayer graphene films by low-pressure diborane-argon plasma, J. Vac. Sci. Technol. A 39 (2021) 043003, https://doi.org/10.1116/6.0000924.

[29] G. Robert Bigras, R. Martel, L. Stafford, Incorporation-limiting mechanisms during nitrogenation of monolayer graphene films in nitrogen flowing afterglows, Nanoscale 13 (2021) 2891–2901, https://doi.org/10.1039/D0NR07827A.

[30] S. Choubak, M. Biron, P.L. Levesque, R. Martel, P. Desjardins, No graphene etching in purified hydrogen, J. Phys. Chem. Lett. 4 (2013) 1100–1103, https://doi.org/10.1021/jz400400u.

[31] A. Reina, H. Son, L. Jiao, B. Fan, M.S. Dresselhaus, Z. Liu, J. Kong, Transferring and identification of single- and few-layer graphene on arbitrary substrates transferring and identification of single- and few-layer graphene on arbitrary substrates, J. Phys. Chem. C 112 (2008) 17741–17744, https://doi.org/10.1021/jp807380s.

[32] A. Roberts, D. Cormode, C. Reynolds, T. Newhouse-Illige, B.J. Leroy, A.S. Sandhu, Response of graphene to femtosecond high-intensity laser irradiation, Appl. Phys. Lett. 99 (2011) 051912, https://doi.org/10.1063/1.3623760.

[33] E.H.M. Ferreira, M.V.O. Moutinho, F. Stavale, M.M. Lucchese, R.B. Capaz, C. A. Achete, A. Jorio, Evolution of the Raman spectra from single-, few-, and many-layer graphene with increasing disorder, Phys. Rev. B 82 (2010) 125429, https://doi.org/10.1103/PhysRevB.82.125429.

[34] M. Bruna, A.K. Ott, M. Ijäs, D. Yoon, U. Sassi, A.C. Ferrari, Doping dependence of the Raman spectrum of defected graphene, ACS Nano 8 (2014) 7432–7441, https://doi.org/10.1021/nn502676g.

[35] R. Fates, R. Remmouche, T. Benkedidah, J. Raskin, Evolution of the Raman spectra features of defective monolayer graphene in back-gate configuration: experimental study, Diam. Relat. Mater. 136 (2023) 109919, https://doi.org/10.1016/j.diamond.2023.109919.

[36] J. Kotakoski, J.C. Meyer, S. Kurasch, D. Santos-Cottin, U. Kaiser, A. V. Krasheninnikov, Stone-Wales-type transformations in carbon nanostructures driven by electron irradiation, Phys. Rev. B Condens. Matter 83 (2011) 245420, https://doi.org/10.1103/PhysRevB.83.245420.

[37] A.K. Manna, S.J. Gilbert, S.R. Joshi, T. Komesu, S. Varma, Effect of topological non-hexagonal rings and Stone Wale defects on the vibrational response of single and multi-layer ion irradiated graphene, Phys. E Low-dimens. Syst. Nanostruct. 143 (2022) 115329, https://doi.org/10.1016/j.physe.2022.115329.

[38] A. Postl, P.P.P. Hilgert, A. Markevich, J. Madsen, K. Mustonen, J. Kotakoski, T. Susi, Indirect Measurement of the Carbon Adatom Migration Barrier on Graphene, Carbon 196 (2022) 596–601.

[39] J. Lin, K. Nishida, M. Saito, First-principles calculations of adatom-vacancy pairs on the graphene, Jpn. J. Appl. Phys. 51 (2012) 125101, https://doi.org/10.1143/JJAP.51.125101.

[40] V.O. Özçelik, H.H. Gurel, S. Ciraci, Self-healing of vacancy defects in single-layer graphene and silicene, Phys. Rev. B Condens. Matter 88 (2013) 045440, https://doi.org/10.1103/PhysRevB.88.045440.

[41] P. Wu, Y. Zhang, P. Cui, Z. Li, J. Yang, Z. Zhang, Carbon dimers as the dominant feeding species in epitaxial growth and morphological phase transition of graphene on different cu substrates, Phys. Rev. Lett. 114 (2015) 216102, https://doi.org/10.1103/PhysRevLett.114.216102.